INVESTIGATION OF BORON AND NITROGEN ION BEAM IMPLANTATION IN GOLD THIN FILMS FOR OHMIC MEMS SWITCH CONTACT IMPROVEMENT

Brice Arrazat, Karim Inal, Patrice Gergaud

INVESTIGATION OF BORON AND NITROGEN ION BEAM IMPLANTATION IN GOLD THIN FILMS FOR OHMIC MEMS SWITCH CONTACT IMPROVEMENT

B. Arrazat[a,b*], K. Inal[c] and P. Gergaud[b]

[a] Ecole Nationale Supérieure des Mines de Saint-Etienne, CMP, 880 route de Mimet, 13541 Gardanne, France
[b] CEA, LETI, MINATEC campus, 17 rue des Martyrs, 38054 Grenoble cedex 9, France
[c] Mines ParisTech, CEMEF - UMR CNRS 7635, 1 rue Claude Daunesse, 06904 Sophia Antipolis, France

ABSTRACT

Contact material and more precisely surface properties are a major issue for RF MEMS ohmic switch reliability. Shallow ion implantation of boron and nitrogen on gold thin film is investigated to increase surface hardness with a limited impact on Electrical Contact Resistance (ECR). The implantation energies were chosen to place the concentration peak of the implanted species at a depth of 100 nm. A microstructural analysis shows that the hardness increases with boron concentration due to a solid solution hardening mechanism, whereas in case of nitrogen, for concentration above 1%, the nitrogen precipitates into a nitride phase correlated to a hardness decrease. The ECR is measured using a Nanoindenter XP which experimental setup reproduces MEMS ohmic switch contact (from 100 µN to 1 mN applied loads under 1 mA). A notable result is obtained with a boron dose of 7.37×10^{16} ions/cm² at 90 keV into gold thin film: 50% hardness increase and 2.6 times higher ECR than pure gold.

INTRODUCTION

RF MEMS ohmic switches have demonstrated higher performances than solid state switches but their reliability represents a major issue for their commercialization [1]. Since the first publication on ohmic MEMS switch [2], gold contact material is diagnosed as main failure reason due to its low hardness [3, 4]. Thus several studies are dedicated to the optimization of the contact material.

Gold alloying ($AuPt_{5\%}Cu_{0.5\%}$ [4], $AuNi_{20\%}$ [5] and $AuRu_{5\%}$ [6]), thin strengthening coatings (Ru and RuO_2 [7, 8]) and Oxide Dispersion Strengthening ($Au-V_2O_5$ 4%vol [9, 10]) provide higher hardness, higher lifetime but Electrical Contact Resistance (ECR) increase compared to pure gold (Fig. 1).
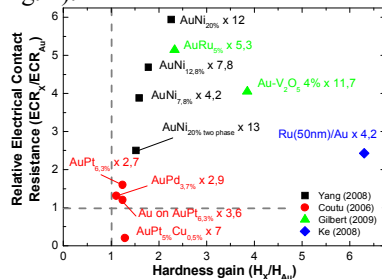

Figure 1: Relative Electrical Contact Resistance (ECR) and lifetime gain plotted as a function of hardness increase regarding pure gold contact [4-10].

Gold concentration must be higher than 80%at (atomic percent) to limit polymer formation in gold - platinum group alloys [11]. Otherwise, a high purity environment is needed [12]. Furtermore, thin protection coatings have limited impact on ECR comparing to other solutions (Fig.

1).

Indeed, in this work, ion beam implantation of boron or nitrogen is investigated as an alternative solution to increase superficial hardness using a small amount of additive (section 1). To compare our work to [4-10], hardness (section 2) and ECR [13] (section 4) are measured using a Nanoindenter XP. To understand hardening mechanisms and the difference between the two species in hardness increase, a microstructural analysis is performed (section 3). The impact on ECR is also analyzed (section 4).

1. ION BEAM IMPLANTATION

Identically to [4-10], a pure gold sample is used as reference and consists of the following sputtered thin film stack deposited on a 8" silicon substrate: 1 µm of pure gold (5N) / 50 nm tungsten nitride diffusion barrier / 20 nm tungsten adhesion layer.

The incident ion beam energy and dose (Table 1) are calculated respectively by SRIM simulations [14] to reach maximal concentration [15] at 100 nm depth (R_p) into pure gold thin film. The strangle range (ΔR_p) is estimated to 100 nm. Thus, approximately 200 nm depths from surface are implanted to form a superficial alloy.

The dose (Table 1) is calculated to investigate few atomic parts per million (ppm) to atomic percent (%). Duration and temperature induced by implantation process are indicated in Table 1.

Table 1: Boron and nitrogen ion implantation setups

Species Energy	Dose (ions/cm²)	Concentration (atomic)	Duration (min)	Temp. (°C)
Boron 90 keV	2.65×10^{12}	3.5 ppm	0.5	20
	2.65×10^{13}	35 ppm	0.5	20
	1.47×10^{14}	200 ppm	0.75	30
	$7,36 \times 10^{14}$	0.1 %	1.5	50
	$7,36 \times 10^{15}$	1%	15	150
	$7,37 \times 10^{16}$	10%	100	180
Nitrogen 130 keV	2.73×10^{12}	3.5 ppm	0.5	20
	2.73×10^{13}	35 ppm	0.5	20
	1.56×10^{14}	200 ppm	0.75	35
	$7,8 \times 10^{14}$	0.1 %	1.5	60
	$7,8 \times 10^{15}$	1%	15	180
	$7,8 \times 10^{16}$	10%	75	250

In the following, the samples are noted Bx or Nx for respectively boron and nitrogen. The index x corresponds to the concentration.
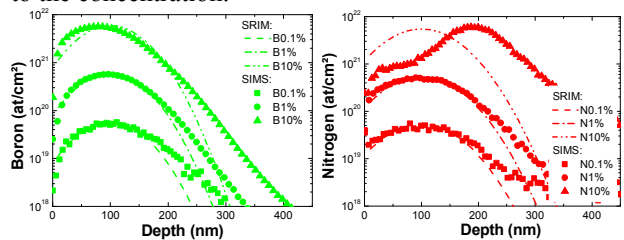

Figure 2: Boron (a) and nitrogen (b) concentration profiles into gold thin film extracted by SIMS.

The boron and nitrogen ions profiles extracted from SIMS are in agreement with SRIM simulations (Fig. 2): R_p is 100 nm and ΔR_p approximately 100 nm, excluding N10%. The former is discussed on section 3.

2. HARDNESS MEASUREMENT

A Nanoindenter XP (MTS Nano Instruments, Knoxville, TN) using the Dynamic Contact Module (DCM) equipped with a Berkovich indenter tip is used to determine the hardness with the Continuous Stiffness Measurement (CSM) technique. The oscillation is 1 nm at a 50 Hz frequency and the strain rate is constant (0.05 s^{-1}). Loubet's theory [16], which considers the pile-up formation during indentation, is used to determine contact depth. The hardness is extracted by Oliver and Pharr method [17]. For each concentration, the average of 64 indentations at 350 nm depth is plotted on Figure 2.
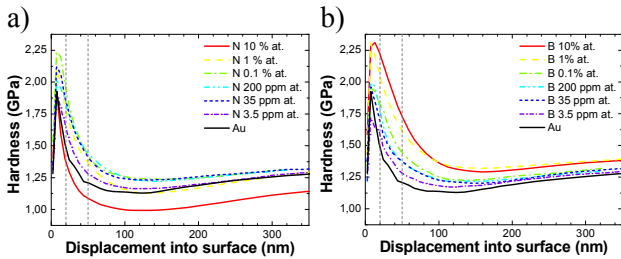

Figure 3: Gold thin film hardness measurement as a function of depth and implantation concentration of nitrogen (a) and boron (b).

The implantation induces hardness variation under small depths as expected (Fig. 3). To highlight the hardness modification due to implantation, the hardness gain is calculated (G_x) and plotted on Figure 4:

$$G_x(\%) = 100 \times \frac{H_x - H_{Au}}{H_{Au}} \quad (1)$$
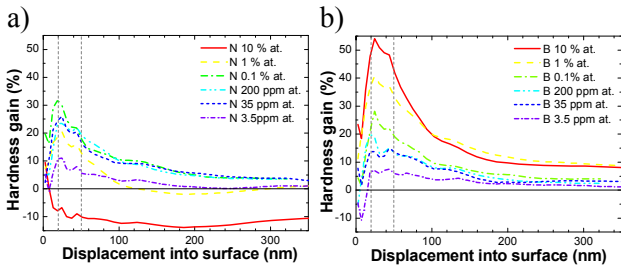

Figure 4: Hardness gain (Eq. 1) as a function of depth and implantation concentration of nitrogen (a) and boron (b).

The boron and nitrogen hardness gain curves (Fig. 4) are similar each other excluding N10% (see section 3). The hardness gain increases from surface to around 20 - 50 nm to reach a maximum. Then, the gain decreases as a function of the depth, and becomes negligible for 300 nm depth. Higher the concentration is, higher the maximum hardness gain is. An analogy could effectively be done on hardness gain curves and ions profiles (Fig. 2).

Indeed, the samples (Table 1) could be summarized as following thin film stack: 200~300 nm of superficial alloy / 700~800 nm of pure gold / silicon substrate. Assuming Bückle hypothesis [18], the hardness of superficial alloy can be extracted at 10% of its depth (let 20~30 nm). Thus, an average of hardness gain is

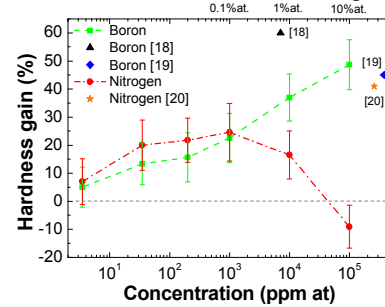calculated between 20 and 50 nm for both species (Fig. 5).

Figure 5: Hardness gain (Eq. 1) as a function of nitrogen and boron concentration calculated between 20 and 50 nm depth.

In the case of boron, the hardness increases with concentration increase. A maximum of 50% hardness increase is reached for an atomic concentration of 10%.

This gain is totally coherent with literature: a gain of 60% is reached by Uchiyama with boron 0.7%at [19]. A hardness gain of 45% is reached in palladium with boron 38%at (18.5, 6.5, 3.2 and 2.3 x 10^{16} ions/cm^2 at respectively 150, 75, 45, and 25 keV) [20].

The evolution of hardness gain is similar for both species from 3.5 ppm to 0.1%. Then, the hardness gain of nitrogen decreases with the increase of concentration. A hardness gain of 41% is reached in palladium with nitrogen 26%at (2 x 10^{17} ions/cm^2 at 100 keV) [21]. No similar gain is reached in our case.

To understand hardening mechanisms and the difference between the two species in hardness gain, a microstructural analysis is performed.

3. MICROSTRUCTURAL ANALYSIS

As presented before, boron and nitrogen ions profiles extracted from SIMS are in agreement with SRIM simulations, except for the case of N10%, which exhibit a deeper R_p of 200 nm. As in hardness measurement, this sample is largely different from the others. Indeed, N10% has the longer process duration and higher temperature reached (see Table 1), inducing probably an additional strong microstructure variation.

In order to explain this variation, Grazing Incidence X-Ray Diffraction (GI-XRD), Electron BackScattered Diffraction (EBSD) and Atomic Force Microscopy (AFM) are performed.

No modification of the crystallographic texture is induced by implantation. The {111} fiber texture, measured by EBSD, is conserved on all samples. The average grain (deduced from EBSD analysis) size increases with the temperature reached during implantation process (Fig. 6). The same evolution is measured for both species. In the case of nitrogen, the average grain size increases from 115 nm to 230 nm. N10% has the higher average grain size due to its higher temperature reached during implantation process.

As comparison, a thermal annealing at 300°C during 1 hour is realized on the pure gold thin film. The measured average grain size increases from 115 nm to 325 nm. The grain size increase due to implantation process is similar to a "classical" annealing. Thus, the EBSD analysis reveals a grain growth for both species due to the temperature
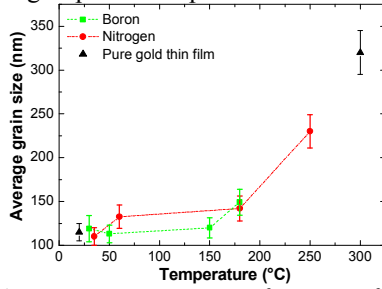
reached during implantation process.

Figure 6: Average grain size as a function of temperature reached during implantation process. Results for pure gold thin film corresponds to an annealing

GI-XRD reveals two new diffraction peaks respectively close to {200} and {400} peaks of pure gold only for N10% (Fig. 7). These peaks could be due to another crystalline phase with a lattice parameter close to pure gold.
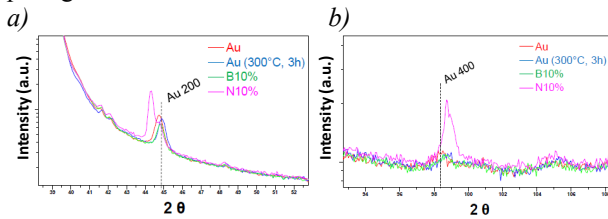

Figure 7: X-ray θ-2θ diffractograms of pure gold thin film (Au), 10%at boron (B10%) and 10%at nitrogen (N10%) focused on 200 (a) and 400 (b) gold crystal peaks.

N10% presents two populations of grain on AFM image (Fig. 8). The first one is around 250 nm grain size as measured by EBSD. The second has a grain size in 30-80 nm range and looks like small "clusters" (Fig. 8 - circled). This type of small "clusters" is exclusively present on N10%. Coupling AFM, GI-XRD and results from [22], it is assumed that small "clusters" are nitride precipitates.
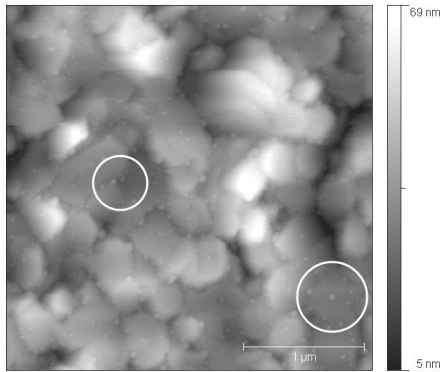

Figure 8: AFM image 3 x 3 µm² of 10%at nitrogen. Some "clusters" are white circled.

Using the previous results, the following scenario of hardening mechanism is proposed. Assuming Hume-Rothery rules, both boron and nitrogen ions are inserted to tetrahedral and octahedral sites of FCC gold crystal. Concerning boron, the hardness increases with concentration (Fig. 5) by solid solution hardening. The same applies to nitrogen when the concentration is lower than 1%. For higher nitrogen concentration, the nitrogen atoms leave insertion sites to precipitate into a nitride

phase, so that the solid solution hardening effect decreases.

The gold nitride is well-known to be harder than pure gold [23]. In our case, the gold nitride precipitates in a soft gold matrix. Furthermore, the gold thin film is softer after implantation due to grain growth (Fig. 6). The precipitate hardening impact depends on dispersion and size of precipitates. In the case of Oxide Dispersion Strengthening, hardening of gold thin film is measured with 3 nm sized particles [9, 10, 24]. The gold nitride precipitates on N10% sample measure 30 − 80 nm range. Thus N10% is softer than pure gold before implantation.

The hardness mechanisms are clearly identified. The link between superficial treatment and microstructure is done. Its effect on Electrical Contact Resistance has to be analyzed.

4. ELECTRICAL CONTACT RESISTANCE

The electrical resistivity is measured but do not allow a good prediction of ECR. To compare our work to [4-10], ECR is measured using a Nanoindenter XP which experimental setup reproduces MEMS ohmic switch contact [13] (from 100 µN to 1 mN applied loads under 1 mA).

An innovative test method developed by M.D. Diop [25] and P.-Y. Duvivier [13] is used for studying ECR by reproducing microswitches geometry. The test structure is constituted by micro bars that are flat on one side and provided with tens of aligned spherical micro bumps on the other one. They are put in contact at low loads in the 100 − 1000 µN range using a Nanoindenter XP, thus enabling direct ECR measurements (Fig. 9). The current applied is 1 mA. The ECR is measured using 4 probes technique.
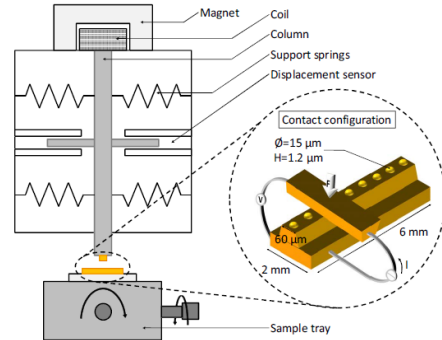

Figure 9: Experimental setup reproducing MEMS ohmic switch contact using a Nano-indenter XP with a zoom on two contacting test specimens [13].

To respect time dependence, the same procedure as [13] is applied and consists of performing measurements of ECR over a long period (5000 s) under constant load. The complete test sequence is presented Fig. 10. As thermal drift of the indentation column is really an issue, two drift measurements are performed at 10 % of maximum load to examine its evolution throughout the test. They always follow unloading segments to minimize creep contribution. The loading / unloading rate is set at 10 µN/s for each test. Adhesion could be observed through the pull-off force necessary to separate the surfaces in the last unloading segment: it is the force at which the separation (S) occurs. Finally, a second contact (C2) is

realized to notice any surface deformation. The approximate duration of the entire testing procedure is 7500 s.
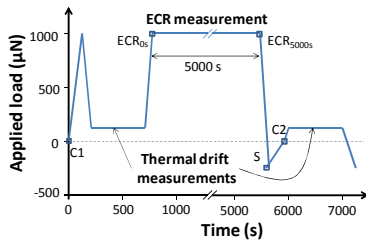

Figure 10: Flowchart of the test procedure for the load applied by Nano-indenter XP over time. C1 represents the first contact and C2 the second. S indicates the separation. The two thermal drift measurement segments last 500 s each while the ECR measurement lasts 5000 s [13].

Each point reported on Fig. 11 corresponds to the ECR at the beginning of ECR measurement (ECR_{0s}). ECR_{0s} of B10% and N10% are slightly higher than pure gold (Fig. 11). Under 100 µN, the ECR_{0s} of B10%, N10% and pure gold thin film are respectively 1.72 Ω, 0.88 Ω and 0.67 Ω.

The harder is the contact material, the higher is the increase of ECR when the load decreases (Fig. 11). The following order (harder to softer) is determined by hardness measurement and confirmed by ECR measurement: B10%, pure gold, N10%. Indeed, ECR depends on the real contact area that is only about a few percent of the apparent contact area under low contact pressure [26]. Real contact area is made of a spatial distribution of contact spots which their size depends on mechanical properties [26]. The harder is the contact material, the smaller is the contact area and so the higher is the ECR.
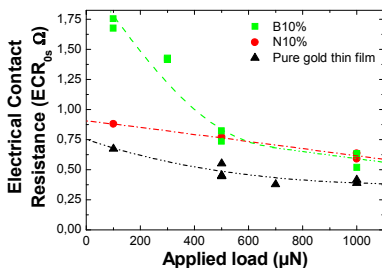

Figure 11: Electrical Contact Resistance at the beginning of measurements (ECR_{0s}) of pure gold thin film, B10% and N10% as a function of applied loads.

After 5000 s of ECR measurement (Fig. 12), the ECR_{5000s} of pure gold, B10% and N10% are quiet similar. The values are in the same range of 250 to 400 mΩ and lower than ECR_{0s}. This ECR decrease corresponds to the creep flow of asperities which yields higher contact spot areas and therefore lower resistance [13]. For all, a slightly increase of ECR is observed as the applied load decreases.
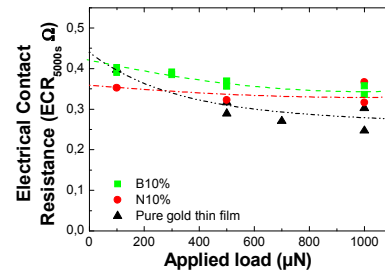

Figure 12: Electrical Contact Resistance at the end of measurements (ECR_{5000s}) of pure gold thin film, B10% and N10 as a function of applied loads.

In the case of N10%at, dark spots are observed on SEM images of contact area after ECR measurements. They could be attributed to carbon presence and therefore shorter lifetime. These dark spots are directly linked to the presence of gold nitride precipitates. It is possible that these nitrides are more resistive than pure gold, and induce higher local current density on contact.

To summarize, the ECR of treated surface are closed to pure gold's ECR as expected.

CONCLUSIONS

In the context of ohmic MEMS switch, the objective is to provide reliable contact material having a small ECR. Thus, a new alternative is proposed to increase superficial hardness using a small amount of additive: ion beam implantation of boron or nitrogen.

Compared to pure gold thin film, increase of 50% superficial hardness and 157% of ECR are obtained through boron implantation dose of 7.37×10^{16} at/cm² at 90 keV (noted B10%).

The microstructural analysis reveals solid solution (by insertion) hardening for boron. The same occurs for nitrogen with concentration under 1%at. In the case of N10%, gold nitride precipitate formation is reported. But SEM analysis after electrical measurement of N10% sample seems to reveal carbon presence and therefore predicts shorter lifetime.

To conclude, B10% achieves success to increase superficial hardness and slightly increase ECR compare to [4-10] (Fig. 13). The initial objective is reached. Shallow ion beam implantation has a respectable place compared to [4-10] (Fig. 13). The proposed sample B10% has the best results from our study and could be interesting to be cycling tested. Other species as calcium, beryllium and barium has demonstrated higher hardness gain [19, 27, 28] and so, should be interesting to investigate.
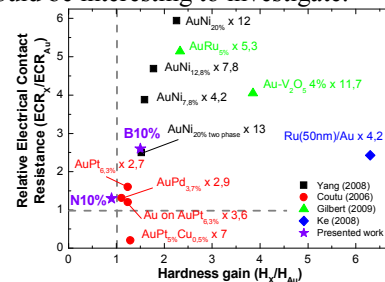

Figure 13: Comparison of presented work and references [4-10] of Relative Electrical Contact Resistance (ECR) and lifetime gain plotted as function of hardness increase regarding pure gold contact.

The increase of hardness is linked to an increase of lifetime, but no direct proportionality exists. Yang *et al.* [5] demonstrate the importance of microstructure: higher lifetime is obtained with a lower hardness gain comparing $AuNi_{20\%}$ and $AuNi_{20\%}$ two-phase. By controlling surface microstructure, contact materials of ohmic MEMS switch can be optimized and tailoring for both mechanical and electrical properties.

ACKNOWLEDGMENTS

REFERENCES

[1]   G. M. Rebeiz. RF MEMS Theory, design, and technology, pages i–v. John Wiley & Sons, Inc., 2003.

[2]   K. E. Petersen. Micromechanical membrane switches on silicon. IBM J. Res. Dev., 23:376–385, 1979.

[3]   B. Arrazat, V. Mandrillon, K. Inal, M. Vincent, and C. Poulain. Microstructure evolution of gold thin films under spherical indentation for micro switch contact applications. J. Mat. Sci., pages 1–7, 2011.

[4]   R. Coutu, J. Reid, R. Cortez, R. Strawser, and P. Kladitis. Microswitches with sputtered au, AuPd, Au-on-AuPt and AuPtCu alloy electric contacts. IEEE Trans. Comp. Pack. Techn., 29(2):341–349, 2006.

[5]   Z. Yang, D. Lichtenwalner, A. Morris, J. Krim, and A. Kingon. Comparison of Au and AuNi alloys as contact materials for MEMS switches. J. Microelectromech. S., 18(2):287–295, 2009.

[6]   K. W. Gilbert, S. Mall, and K. D. Leedy. A nanoindenter based investigation of gold-ruthenium alloy microcontact behavior under cyclic condition. J. Adh. Sci. Tech., 26(8-9):1181–1199, 2012.

[7]   F. Ke, J. Miao, and J. Oberhammer. A ruthenium-based multimetal-contact RF MEMS switch with a corrugated diaphragm. J. Microelectromech. S., 17(6):1447–1459, 2008.

[8]   M. Walker, C. Nordquist, D. Czaplewski, G. Patrizi, N. McGruer, and J. Krim. Impact of in situ oxygen plasma cleaning on the resistance of Ru and Au-Ru based RF microelectromechanical system contacts in vacuum. J. App. P., 107(8):084509, 2010.

[9]   K. W. Gilbert. Investigation into contact resistance and damage of metal contacts used in RF-MEMS switches. PhD thesis, Air Force Institute of Technology, 2009.

[10]   Bannuru, T., S. Narksitipan, W. L. Brown, and R. P. Vinci (2007), Effects of V additions on the mechanical behavior of Au thin films for MEMS contact switches, Vol. 6463, SPIE, p. 646306.

[11]   Chen, L., H. Lee, Z. J. Guo, N. E. McGruer, K. W. Gilbert, S. Mall, K. D. Leedy, and G. G. Adams. Contact resistance study of noble metals and alloy films using a scanning probe microscope test station. J. App. P. 102(7), 074910, 2007.

[12]   Dickrell, D.J. & M.T. Dugger. Silicone oil contamination and electrical contact resistance degradation of low-force gold contacts. J. Microelectromech. S., 16(1),

[13]   P.-Y. Duvivier, V. Mandrillon, K. Inal, C. Dieppedale, S. Deldon-Martoscia, and J. Polizzi. Time dependence investigation of the electrical resistance of Au / Au thin film micro contacts. 56th IEEE Holm Conference on Electrical Contacts, pages 1–7, 2010.

[14]   J. F. Ziegler. SRIM, 2008 version 4.

[15]   M. Nastasi, J. W. Mayer and J. K. Hirvonen. Ion Solid Interaction: Fundamentals and applications. University of Cambridge, 1996.

[16]   J.L. Loubet, M. Bauer, A. Tonck, S. Bec, and B. Gauthier-Manuel. Nanoindentation with a force apparatus. Mechanical Properties and Deformation Behavior of Materials Having Ultra-Fine Microstructures, 429-447, 1993.

[17]   G.M. Pharr, J.H. Strader, and W.C. Oliver. Critical issues in making small-depth mechanical property measurements by nanoindentation with continuous stiffness measurement. J. Mat. Res., 24(3):653–666, 2008.

[18]   H. Bückle, *Metall. Rev.* **4** 49-100, 1959.

[19]   N. Uchiyama . Golden ornament material hardened by alloying with minor components. Patent EP0685565B1, 1995.

[20]   M. Antler, C. Preece, and E. Kaufmann. The effect of boron implantation of the sliding wear and contact resistance of palladium, 60Pd40Ag, and a cousin's alloy. IEEE Transactions on Components, Hybrids, and Manufacturing Technology, 5(1), 81 – 85, 1982.

[21]   P.W. Leech. The tribological properties of N2+ implanted AuAgCu alloy and palladium in sliding contact with gold electroplate. IEEE Transactions on Components, Hybrids, and Manufacturing Technology, 13(2), 353–357, 1990.

[22]   A. C. Brieva, L. Alves, S. Krishnamurthy, and L. Šiller. Gold surface with gold nitride–a surface enhanced Raman scattering active substrate. J. Appl. Phys., 105(5):054302, 2009.

[23]   Siller, L., N. Peltekis, S. Krishnamurthy, Y. Chao, S. J. Bull, and M. R. C. Hunt. Gold film with gold nitride - a conductor but harder than gold. Appl. Phys. Lett. 86(22), 221912, 2005.

[24]   J. R. Williams, and D. R. Clarke. Strengthening gold thin films with zirconia nanoparticles for MEMS electrical contacts. Acta Mat. 56(8), 1813 – 1819, 2008.

[25]   M.D. Diop, V. Mandrillon, H. Boutry, K. Inal, and R. Fortunier. Analysis of nickel cylindrical bump insertion into aluminium thin film for flip chip applications. Micro. Eng., Volume 87, Issue 3, March 2010, Pages 522–526.

[26]   B. Arrazat, P.-Y. Duvivier, V. Mandrillon, and K. Inal. Discrete analysis of gold surface asperities deformation under spherical nano-indentation towards electrical contact resistance calculation. 57th IEEE Holm Conference on Electrical Contacts, pages 1 – 8, 2011.

[27]   E. Asada, K. Yokoyama, M. Yata, and K. Hirano. Bonding wire. US Patent 4752442, 1988.

[28]   T. S.Saraswati, T. Sritharan, C. I. Pang, Y. H. Chew, C. D. Breach, F. Wulff, S. G. Mhaisalkar and C. C. Wong. The effects of Ca and Pd dopants on gold bonding wire and gold rod. Thin Solid Films 462-463, 351 – 356, 2003.